nature materials

LETTERS

PUBLISHED ONLINE: 24 NOVEMBER 2013 | DOI: 10.1038/NMAT3804

Enhancing multiphoton upconversion through energy clustering at sublattice level

Juan Wang[1†], Renren Deng[1†], Mark A. MacDonald[2], Bolei Chen[3], Jikang Yuan[3], Feng Wang[4], Dongzhi Chi[4], Tzi Sum Andy Hor[1,4], Peng Zhang[2], Guokui Liu[5], Yu Han[6] and Xiaogang Liu[1,4]*

The applications of lanthanide-doped upconversion nanocrystals in biological imaging, photonics, photovoltaics and therapeutics have fuelled a growing demand for rational control over the emission profiles of the nanocrystals[1–14]. A common strategy for tuning upconversion luminescence is to control the doping concentration of lanthanide ions[15,16]. However, the phenomenon of concentration quenching of the excited state at high doping levels poses a significant constraint. Thus, the lanthanide ions have to be stringently kept at relatively low concentrations to minimize luminescence quenching[17]. Here we describe a new class of upconversion nanocrystals adopting an orthorhombic crystallographic structure in which the lanthanide ions are distributed in arrays of tetrad clusters. Importantly, this unique arrangement enables the preservation of excitation energy within the sublattice domain and effectively minimizes the migration of excitation energy to defects, even in stoichiometric compounds with a high Yb^{3+} content (calculated as 98 mol%). This allows us to generate an unusual four-photon-promoted violet upconversion emission from Er^{3+} with an intensity that is more than eight times higher than previously reported. Our results highlight that the approach to enhancing upconversion through energy clustering at the sublattice level may provide new opportunities for light-triggered biological reactions and photodynamic therapy.

For an efficient upconversion to proceed, trivalent Yb^{3+} ions are typically doped in nanocrystals as sensitizers together with Er^{3+}, Tm^{3+} and Ho^{3+} activators[1]. An elevated amount of Yb^{3+} content is likely to enhance the luminescence efficiency of upconversion as the Yb^{3+} ion has a sufficient absorption cross-section matched to common 980-nm laser excitation sources. However, appreciable quenching of luminescence, particularly in the spectral region of short wavelengths, is experimentally observed for upconversion nanocrystals with high doping levels (typically greater than 20 mol%) of Yb^{3+} (ref. 18). Despite enormous research efforts, the synthesis of upconversion nanoparticles that emit intense short-wavelength emission remains an arduous task. One underlying problem is thought to be the inability of most systems containing high Yb^{3+} contents to sustain multi-step excitation without depletion of the intermediate excited states.

The depletion of excitation energy in upconversion nanocrystals with a high Yb^{3+} content is most likely due to an increased probability of long-distance energy migration that takes excitation energy to lattice or surface defects. This phenomenon has been frequently observed in Yb^{3+}-doped nanocrystals featuring high-symmetry unit cells (for example, cubic-phase $NaYF_4$ and CaF_2; refs 19,20) that promote the dissipation of the excitation energy in the presence of isotropically substituted Yb^{3+} ions (Fig. 1, type I). Other pathways of deleterious energy migration can occur through either two-dimensional (2D) layered structures (for example, $NaEuTiO_4$ for Eu^{3+}–Eu^{3+} energy migration)[21] or

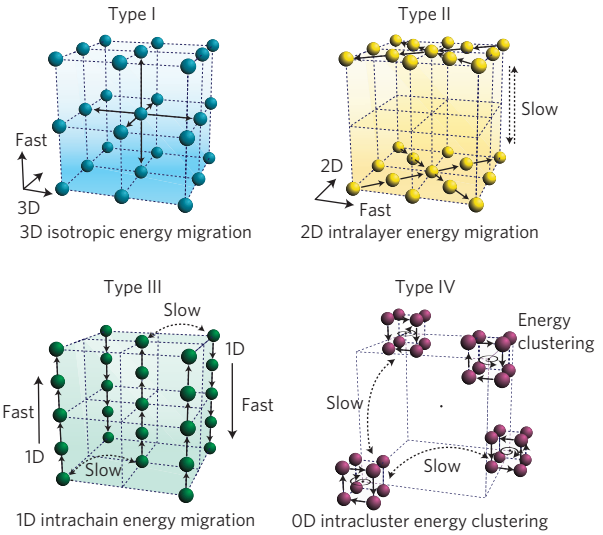

Figure 1 | Schematic representation showing the topological energy migration pathways in different types of crystal sublattice. The type I scheme represents the random energy migration from an atom to its neighbouring atoms isotropically distributed in a 3D structured crystal sublattice. The type II scheme shows the energy migration in a crystal with a 2D layer structure. The type III scheme refers to the energy migration in a crystal featuring a 1D atomic chain structure. Note that in schemes of type II and III, fast energy migration only occurs through in-plane atoms and chain lattices, respectively. The migration of excitation energy can be effectively minimized through use of a type IV lattice containing arrays of isolated atomic clusters. As such, they allow the trapping of the excitation energy in discrete sublattices through energy clustering. The energy migration between adjacent clusters is unfavourable owing to the relatively long distances.

[1]Department of Chemistry, National University of Singapore, Singapore 117543, Singapore, [2]Department of Chemistry, Dalhousie University, Halifax, Nova Scotia B3H 4J3, Canada, [3]Department of Applied Physics, The Hong Kong Polytechnic University, Kowloon, Hong Kong, [4]Institute of Materials Research and Engineering, Agency for Science, Technology and Research, Singapore 117602, Singapore, [5]Argonne National Laboratory, Chemical Sciences and Engineering Division, Argonne, Illinois 60439, USA, [6]Advanced Membrane and Porous Materials Center, Physical Science and Engineering Division, King Abdullah University of Science and Technology, Thuwal 23955-6900, Saudi Arabia. †These authors contributed equally to this work.
*e-mail: chmlx@nus.edu.sg

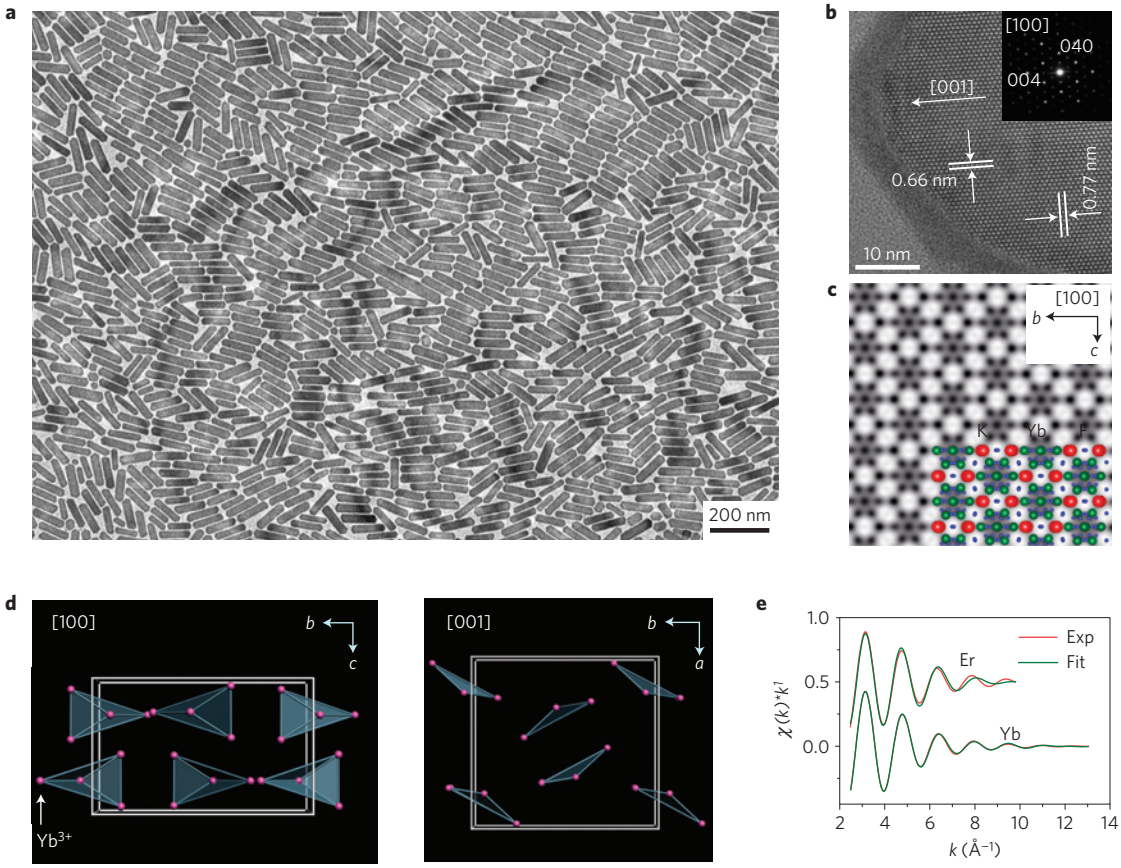

Figure 2 | Structural characterization of the as-synthesized KYb_2F_7:Er (2 mol%) nanocrystals. a, Typical low-resolution TEM micrograph of the nanocrystals. **b**, High-resolution TEM image of a single nanocrystal and its corresponding selected-area electron diffraction pattern (inset) taken in [100] incidence. **c**, Projected potential map of the high-resolution TEM image shown in **b**, which is superimposed by the structural model of KYb_2F_7 projected along the [100] direction for comparison. **d**, Schematic representation of the lattice arrangement of Yb atoms in orthorhombic-phase KYb_2F_7 viewed from the [100] and [001] planes, respectively. Arrays of discrete Yb clusters are highlighted as grey tetrahedrons for clarity. **e**, Experimental (Exp) and fitted (Fit) Ln–F shell extended X-ray absorption fine structure spectra in k^1-space of Er and Yb for KYb_2F_7:Er (2 mol%) nanocrystals.

1D chain crystal lattices ($EuMgB_5O_{10}$ for Eu^{3+}–Eu^{3+} energy migration, and Sr_2CeO_4 for Ce^{4+}–O^{2-} charge transfer)[22,23] with in-plane or chain-lattice substituted doping ions situated in close proximity (Fig. 1, types II and III). On the basis of these findings, we recognize that the energy migration process essentially depends on the distance between lattice positions occupied by Yb^{3+} rather than the doping concentration. Therefore, it is possible to minimize the concentration quenching of luminescence through use of a crystal lattice disfavouring long-distance energy migration (Fig. 1, type IV). This is principally applicable if the Yb^{3+} ions are separated as arrays of discrete clusters at the sublattice level in which the averaged distance between the ionic clusters is substantially larger than the ionic distance within the clusters. The clustered structure is able to promote localized energy exchange interaction and simultaneously minimize the delocalization of the excitation energy[24]. Here we report the synthesis and characterization of KYb_2F_7:Er upconversion nanocrystals with lanthanide ions arranged in tetrad clusters. We demonstrate how control over the arrangement of sublattices can be used to tune the energy migration. Our mechanistic investigation, corroborated by theoretical calculations, shows for the first time a four-photon upconversion for violet emission resulting from fast energy transfer within the tetrad Yb clusters.

In our experiment, KYb_2F_7:Er (2 mol%) nanocrystals were synthesized by a co-precipitation method (see Supplementary Information). The X-ray powder diffraction pattern of the as-synthesized sample can be well indexed to an orthorhombic-phase KYb_2F_7 structure (space group *Pnam*, $a = 11.72$ Å, $b = 13.24$ Å, $c = 7.74$ Å, $Z = 8$; Supplementary Fig. 1). A representative transmission electron microscopy (TEM) image reveals an ice lolly stick shape of the nanocrystals. These nanocrystals are 109 nm long, 26 nm wide and 12 nm thick on average (Fig. 2a and Supplementary Fig. 2). The high-resolution TEM image of an individual nanocrystal, taken along the [100] zone axis as shown in Fig. 2b, exhibits lattice fringes of the (020) and (001) planes with a d-spacing of 0.66 nm and 0.77 nm, respectively. The selected-area electron diffraction patterns along with the TEM analysis of the nanocrystal confirm its growth direction along the c axis (Fig. 2b). Processing of the high-resolution TEM image with contrast transfer function correction followed by imposing symmetry leads to a projected potential map (Supplementary Figs 3 and 4), which matches well with the structural model projection for the orthorhombic KYb_2F_7 phase (Fig. 2c). In the orthorhombic phase of KYb_2F_7, the Yb atoms form an array of discrete tetrahedra as highlighted in Fig. 2d. The extended X-ray absorption fine structure results show that the average first shell coordination number for lanthanides is around eight, consistent with the crystal structure of orthorhombic KYb_2F_7, indicating a homogeneous distribution of Er^{3+} dopants in the KYb_2F_7 host lattice (Fig. 2e and Supplementary Table 1). Compositional analysis of the nanocrystal by energy-dispersive X-ray spectroscopy reveals the presence of elements K, Yb and Er (Supplementary Fig. 8).

Figure 3a shows a representative luminescence spectrum of KYb_2F_7:Er (2 mol%) nanocrystals on excitation with a 980-nm diode laser. We observed a set of emission bands corresponding to

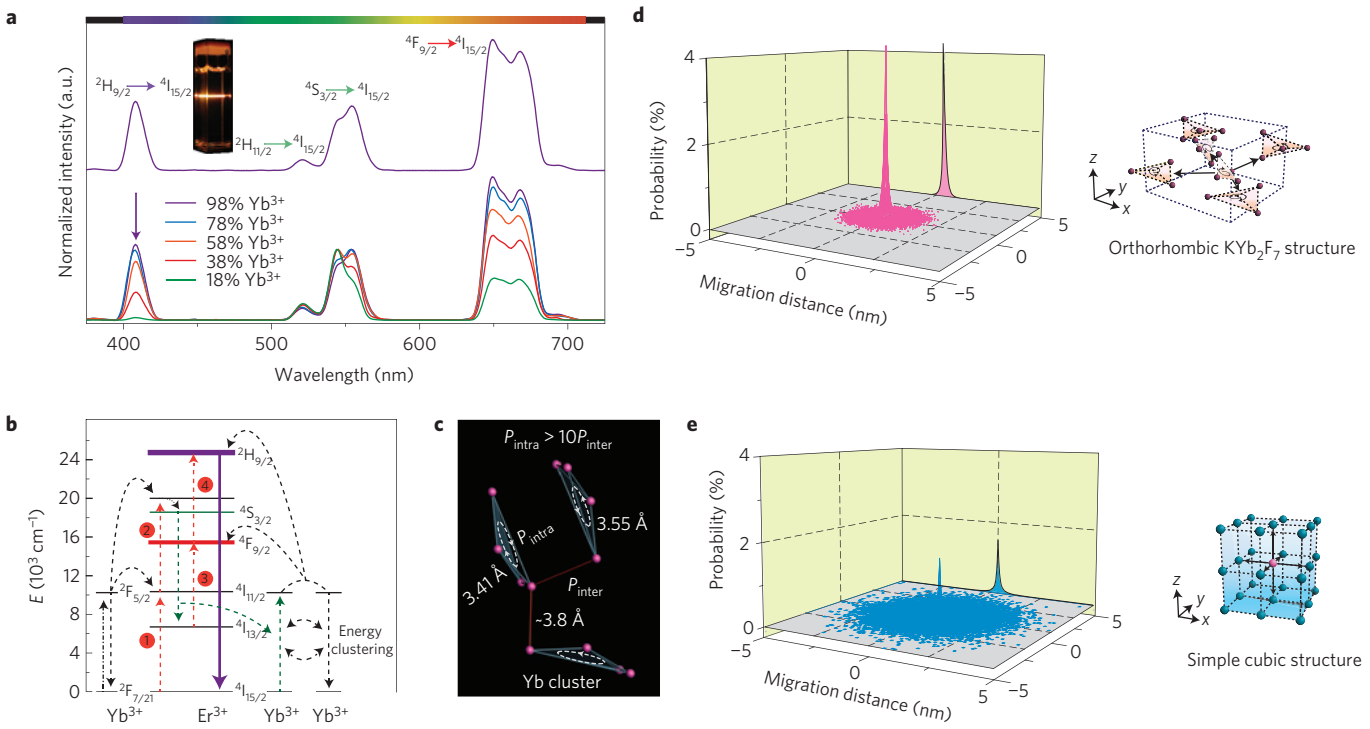

Figure 3 | Optical characterization of the as-synthesized KYb_2F_7:Er nanocrystals. a, Room-temperature (25 °C) emission spectra of KYb_2F_7:Er (2 mol%) (top) and KYb_2F_7:Er/Lu (2/0–80 mol%; bottom) nanocrystals recorded in cyclohexane solutions (0.2 wt%). All samples were excited with a 980-nm laser illumination at a power density of 10 W cm^{-2}. The emission spectra were normalized to Er^{3+} emission either at 558 nm or 545 nm, whichever is stronger. The inset is a typical micrograph showing the luminescence of KYb_2F_7:Er (2 mol%) nanocrystals. **b**, Proposed four-photon upconversion mechanisms in KYb_2F_7:Er nanocrystals following excitation with a 980-nm laser. The $^4S_{3/2}$ state of Er^{3+} is first populated by sequential energy transfer of two photons from an excited Yb^{3+} ion. The $^4I_{13/2}$ state of Er^{3+} is then populated by back-energy-transfer from the $^4S_{3/2}$ state of Er^{3+} to the ground state of a neighbouring Yb^{3+} ion. Subsequently, localized energy transfer within the Yb tetrad cluster provides two additional photons to the Er^{3+} ion, thereby leading to the population of the $^2H_{9/2}$ state. The dashed-dotted, dashed, dotted and full arrows represent photon excitation, energy transfer, multiphonon relaxation, and emission processes, respectively. Note that the multiphoton pumping processes are numbered and highlighted in red. **c**, Proposed excitation energy clustering in the Yb tetrad clusters of orthorhombic-phase KYb_2F_7. The probability of energy transfer within the Yb cluster (P_{intra}) is calculated to be more than 10 times higher than that of inter-cluster energy transfer (P_{inter}). **d**,**e**, The probability of finding the excitation energy plotted against migration distance using Monte Carlo simulations for a KYb_2F_7 crystal (**d**) and a simple cubic structure (**e**). The data sets were constructed by calculating the position of the excitation energy after five thousand steps of nearest-neighbour random walk in two different models.

$^2H_{9/2} \rightarrow {}^4I_{15/2}$ (violet), $^2H_{11/2}$, $^4S_{3/2} \rightarrow {}^4I_{15/2}$ (green), and $^4F_{9/2} \rightarrow {}^4I_{15/2}$ (red) transitions of Er^{3+}. Notably, the intensity ratio of violet-to-green emission is about one order of magnitude larger than that observed for conventional Er^{3+}-doped nanocrystals. To examine the effect of doping composition on emission, we further synthesized a series of nanocrystals with Yb^{3+} partially replaced by optically inactive Lu^{3+} (0–80 mol%). Lu^{3+} was chosen because of its very similar ionic radius and comparable chemical property to Yb^{3+} (ref. 25). Indeed, the as-prepared nanocrystals with different content levels of Lu^{3+} were found to have similar particle size distributions (Supplementary Fig. 9). However, we observe a gradual decrease in the violet-to-green emission ratio with the decrease in Yb^{3+} concentration (98–18 mol%; Fig. 3a). Significantly, we observe no clear differences in the overall integrated emission intensity between these samples (Supplementary Fig. 10), indicating the absence of the concentration quenching effect. This stands in stark contrast to the luminescence quenching observed from conventional systems with high Yb^{3+} content levels, such as $NaYbF_4$:Er (2 mol%) and $LiYbF_4$:Er (2 mol%) nanoparticles (Supplementary Fig. 14). To exclude the impact of particle size and morphology on emission, we also synthesized KYb_2F_7:Er (2 mol%) nanocrystals of different sizes and shapes (Supplementary Fig. 15). The violet-to-green emission ratios of these controls were found to be virtually identical.

We attribute the large increase in violet upconversion emission to the enhanced energy exchange interaction between Yb^{3+} and Er^{3+} at a high Yb^{3+} concentration and confined energy transfer in Yb^{3+} clusters. In conventional Yb^{3+}/Er^{3+} co-doped nanocrystals, the $^4S_{3/2}$ state of Er^{3+} can be easily populated by a Yb-assisted two-photon energy transfer upconversion process[17]. We argue that an elevated level of Yb^{3+} can further induce a back-energy-transfer from the $^4S_{3/2}$ state of Er^{3+} to the $^2F_{7/2}$ state of a nearby Yb^{3+}, resulting in increased populations of the $^4I_{13/2}$ state of Er^{3+} (ref. 15). Subsequent energy transfer in the third and fourth steps from the excited Yb^{3+} to Er^{3+} will populate the $^4F_{9/2}$ and $^2H_{9/2}$ states by three- and four-photon upconversion processes, respectively, eventually leading to the enhanced red and violet emission (Supplementary Fig. 12 and Fig. 3b). This is supported by excitation power-dependent studies where the strong violet upconversion emission was determined to be a four-photon upconversion process in KYb_2F_7 (Supplementary Fig. 11). In sharp contrast, the violet emission of conventional $NaYbF_4$:Er (2 mol%) and $NaYF_4$:Yb/Er (18/2 mol%) nanocrystals was found to be a three-photon process[17], with a decrease in peak intensity by a factor of ~100 and ~8, respectively. Taken together, these data unambiguously suggest the critical role of energy clustering in preserving excitation energy during the upconversion process.

The energy transfer process can be further validated by luminescence decay studies. On increasing the Yb^{3+} concentration from 18 to 98 mol%, we observed only a small decrease in the $^2F_{5/2}$ lifetime of Yb^{3+} from 327 to 223 μs in KYb_2F_7 nanocrystals. This is in stark

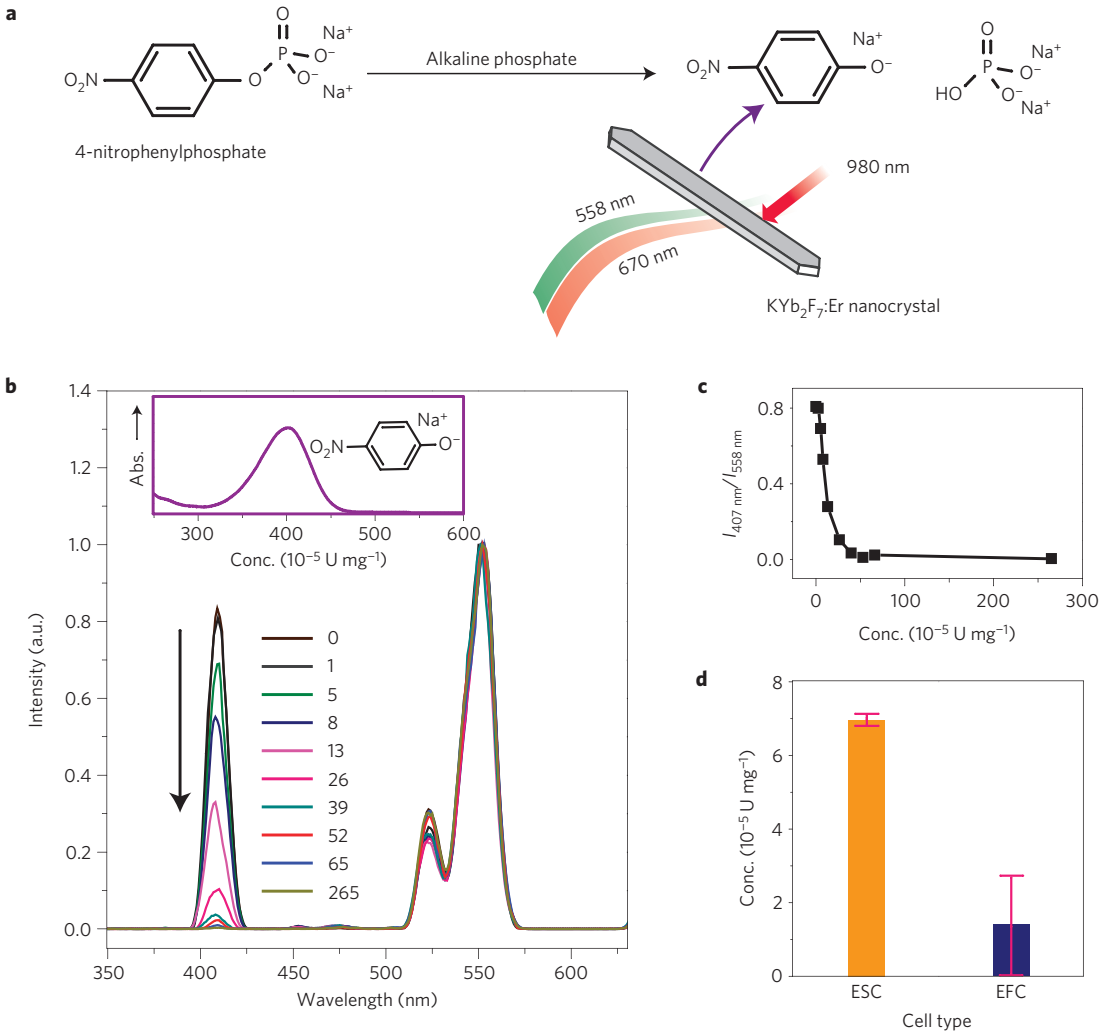

Figure 4 | Enzyme activity screening using the KYb_2F_7:Er (2 mol%) nanocrystals. a, Schematic design for screening the activity of alkaline phosphatase. The enzyme reacts with 4-nitrophenylphosphate to generate 4-nitrophenolate and inorganic phosphate compounds. The resulting 4-nitrophenolate is then transferred into a solution of KYb_2F_7:Er nanocrystals. When irradiated with a 980-nm laser, the nanocrystals exhibit suppressed emission at 407 nm due to a high molar absorptivity of the 4-nitrophenolate at 405 nm. **b**, The emission spectra of nanocrystal solutions containing different amounts of alkaline phosphatase in the presence of 4-nitrophenylphosphate. **c**, The emission intensity ratio ($I_{407\,nm}/I_{558\,nm}$) dependence on enzyme concentration. **d**, Demonstration of alkaline phosphatase detection in mouse embryonic stem cells (ESCs) and embryonic fibroblast cells (EFCs) by combining KYb_2F_7:Er nanocrystals with 4-nitrophenylphosphate. The error bars correspond to standard deviation and are based on $n = 3$ independent experiments.

contrast to the significant decrease in the $^2F_{5/2}$ lifetime of Yb^{3+} from 484 to 33.2 µs in conventional hexagonal-phased $NaYbF_4$ nanocrystals (Supplementary Fig. 13). Thus, a key unanswered question is how the depletion of excitation energy in a lattice of high Yb concentration is minimized in the case of KYb_2F_7 nanocrystals.

To gain insight into the mechanisms responsible for the enhanced upconversion luminescence, we employed a random-walk model to investigate the energy migration between Yb^{3+} ions. On the basis of synchrotron X-ray absorption spectroscopic measurements indicating the presence of Yb–Yb bonding in the range of 3–4 Å (Supplementary Fig. 6), we assumed that the Yb–Yb energy migration is dominated by electric exchange interaction because of the orbital overlap between neighbouring Yb^{3+} ions. Thus, the probability of energy transfer P_{ET} between two adjacent Yb neighbours can be expressed as:

$$P_{ET} = C_{Yb-Yb}\exp(-2R/L)$$

where R is the distance between the energy donor–acceptor pair, C_{Yb-Yb} is the Yb–Yb interaction constant, and L is the effective Bohr radius (estimated to be ~0.3 Å for Yb–Yb interaction[25]). Clearly, the rate of energy transfer between the Yb^{3+} ions is highly dependent on the distance. The increase in the ionic distance will significantly slow down the energy migration among the lanthanide ions, as supported by previous theoretical and experimental investigations[26,27]. Considering the short distance between two neighbouring Yb^{3+} ions within the tetrad cluster (3.41–3.55 Å) and the relatively long distance (3.75–3.83 Å) between the Yb clusters, we conclude that the probability of energy transfer within the Yb cluster (P_{intra}) is more than ten times higher than that of inter-cluster energy transfer (P_{inter}; Fig. 3c). A more plausible origin would be energy transfer confined within the tetrad Yb^{3+} cluster accounting for the observed luminescence enhancement, rather than energy migration through discrete Yb clusters.

We next performed Monte Carlo simulations to describe the migration of excitation energy in different crystal sublattices. The energy migration process in different crystal structures can be differentiated by comparing the probability of energy migration through the host lattice. When absorbed by an Yb^{3+} ion, the excitation energy is able to migrate through the lattice within

its lifetime. To estimate the distance of energy migration, we considered that the excitation energy migrates through the Yb sublattice for five thousand steps of nearest-neighbour random walk before relaxation. As anticipated, the probability of finding excitation energy in the starting point of energy migration after the random walk decreases substantially in a simple cubic structure as contrasted with that in a KYb_2F_7 host lattice (Fig. 3d,e).

To verify the energy clustering effect of the Yb sublattice on activator emission, we examined KYb_2F_7 nanocrystals doped with varying concentrations of Lu^{3+} (0–80 mol%), in combination with Tm^{3+} (0.2 mol%) or Ho^{3+} (2 mol%) activators. Remarkably, the total integrated emission intensities of Tm^{3+} and Ho^{3+} activators were found to be independent of Yb^{3+} concentration (Supplementary Fig. 16). This result strongly implies the absence of long-distance energy migration in the KYb_2F_7 host lattice. The intense upconversion emission resulting from higher-lying states of the activators (for example, the $^1D_2$ state of Tm^{3+} and the $^5F_4$ state of Ho^{3+}) at elevated Yb^{3+} concentrations can be ascribed to an enhanced energy transfer from Yb^{3+} to Tm^{3+} and Ho^{3+}, which is in accordance with that observed for the Er^{3+} activator.

The availability of intense violet upconversion emission from KYb_2F_7:Er nanocrystals offers unique opportunities for the development of integrated biodetection systems. As a proof of concept, we showed that these nanocrystals allow for screening alkaline phosphatases that have been commonly used to diagnose bone and hepatic diseases[28]. The basic design involves measuring luminescence quenching in violet emission of KYb_2F_7:Er nanocrystals when the nanocrystals are brought close to 4-nitrophenolate (Fig. 4a). The 4-nitrophenolate formed by an alkaline phosphatase-catalysed reaction shows a characteristic absorption band centred at 400 nm, overlapping with the violet emission peak of the nanocrystals. As shown in Fig. 4b,c, the violet emission intensity of the upconversion nanocrystals gradually decreased with increasing concentration of alkaline phosphatase. Our approach permits the detection of enzyme activity down to an enzyme concentration of 1×10^{-5} U mg^{-1} after incubation for only 5 min. In contrast to conventional fluorescence-based assays reliant on organic fluorphores[29] or quantum dots[30], our approach provides a multitude of advantages, including much reduced background fluorescence, superior detection sensitivity and fast response time. It should be noted that utilization of near-infrared excitation enables the monitoring of alkaline phosphatase activity directly in a cell culture medium or in cytoplasm without cell isolation and purification (Fig. 4d).

Our experimental work performed on orthorhombic KYb_2F_7:Er nanocrystals indicates an alternative method for tuning upconversion emission. The investigation of enhanced upconversion luminescence through the clustering of excitation energy at the subunit-cell level enables an improved understanding of multiphoton upconversion in nanostructured materials. This study also raises the possibility of constructing high-quality upconversion nanocrystals with desirable optical properties that may outperform conventional fluorescent biomarkers[31].

Methods

Nanocrystal synthesis. Lanthanide-doped KYb_2F_7 nanocrystals capped with oleic acid ligands were grown by a modified literature method according to ref. 32. Further experimental details are provided in the Supplementary Information.

Physical characterization. Low-resolution TEM images were carried out on a JEOL 2010 TEM operating at an acceleration voltage of 200 kV. High-resolution TEM was performed on an FEI Titan S-Twin TEM operated at 300 kV. Powder X-ray diffraction data were recorded on a Siemens D5005 X-ray diffractometer with Cu Kα radiation ($\lambda = 1.5406$ Å) at a scan rate of 0.01° s^{-1}. Photoluminescence spectra were recorded at room temperature with a DM150i monochromator equipped with a R928 photon-counting photomultiplier tube, in conjunction with a 980-nm diode laser. The decay curves were measured by a customized phosphorescence lifetime spectrometer (FSP920-C, Edinburgh) equipped with a digital oscilloscope (TDS3052B, Tektronix) and a tunable mid-band optical parametric oscillator laser as an excitation source (410–2,400 nm, Vibrant 355II, OPOTEK). The effective lifetimes were determined by

$$\tau_{\mathrm{eff}} = \frac{1}{I_0}\int_0^\infty I(t)\,\mathrm{d}t$$

where I_0 and $I(t)$ represent the maximum luminescence intensity and luminescence intensity at time t after cutoff of the excitation light, respectively. The absolute upconversion quantum yields were measured by a steady-state and phosphorescence lifetime spectrometer (FSP920, Edinburgh) coupled with an integrating sphere (150 mm; internally coated with barium sulphate) and a 980-nm diode laser. The absorption spectra were recorded with an ultraviolet–visible–near-infrared spectrophotometer (UV-3600, Shimadzu).

Received 30 June 2013; accepted 7 October 2013; published online 24 November 2013

References

1. Haase, M. & Schäfer, H. Upconverting nanoparticles. *Angew. Chem. Int. Ed.* **50,** 5808–5829 (2011).
2. Zou, W., Visser, C., Maduro, J. A., Pshenichnikov, M. S. & Hummelen, J. C. Broadband dye-sensitized upconversion of near-infrared light. *Nature Photon.* **6,** 560–564 (2012).
3. Zhang, F. *et al.* Direct imaging the upconversion nanocrystal core/shell structure at the sub-nanometre level: Shell thickness dependence in upconverting optical properties. *Nano. Lett.* **12,** 2852–2858 (2012).
4. Wang, F. *et al.* Simultaneous phase and size control of upconversion nanocrystals through lanthanide doping. *Nature* **463,** 1061–1065 (2010).
5. Park, Y. I. *et al.* Comparative study of upconverting nanoparticles with various crystal structures, core/shell structures, and surface characteristics. *J. Phys. Chem. C* **117,** 2239–2244 (2013).
6. Zhao, J. *et al.* Upconversion luminescence with tunable lifetime in $NaYF_4$:Yb,Er nanocrystals: Role of nanocrystal size. *Nanoscale* **5,** 944–952 (2013).
7. Hao, J., Zhang, Y. & Wei, X. Electric-induced enhancement and modulation of upconversion photoluminescence in epitaxial $BaTiO_3$:Yb/Er thin films. *Angew. Chem. Int. Ed.* **50,** 6876–6880 (2011).
8. Wang, F. *et al.* Tuning upconversion through energy migration in core–shell nanoparticles. *Nature Mater.* **10,** 968–973 (2011).
9. Kolesov, R. *et al.* Optical detection of a single rare-earth ion in a crystal. *Nature Commun.* **3,** 1029 (2012).
10. Liu, Y. *et al.* Amine-functionalized lanthanide-doped zirconia nanoparticles: Optical spectroscopy, time-resolved FRET biodetection and targeted imaging. *J. Am. Chem. Soc.* **134,** 15083–15090 (2012).
11. Chen, D., Lei, L., Yang, A., Wang, Z. & Wang, Y. Ultra-broadband near-infrared excitable upconversion core/shell nanocrystals. *Chem. Commun.* **48,** 5898–5900 (2012).
12. Ye, X. *et al.* Morphologically controlled synthesis of colloidal upconversion nanophosphors and their shape-directed self-assembly. *Proc. Natl Acad. Sci. USA* **107,** 22430–22435 (2010).
13. Chen, G., Ohulchanskyy, T. Y., Kumar, R., Agren, H. & Prasad, P. N. Ultrasmall monodisperse $NaYF_4$:Yb^{3+}/Tm^{3+} nanocrystals with enhanced near-infrared to near-infrared upconversion photoluminescence. *ACS Nano* **4,** 3163–3168 (2010).
14. Gorris, H. H. & Wolfbeis, O. S. Photon-upconverting nanoparticles for optical encoding and multiplexing of cells, biomolecules, and microspheres. *Angew. Chem. Int. Ed.* **52,** 3584–3600 (2013).
15. Chan, E. M. *et al.* Combinatorial discovery of lanthanide-doped nanocrystals with spectrally pure upconverted emission. *Nano Lett.* **12,** 3839–3845 (2012).
16. Wang, F. & Liu, X. Upconversion multicolor fine-tuning: Visible to near-infrared emission from lanthanide-doped $NaYF_4$ nanoparticles. *J. Am. Chem. Soc.* **130,** 5642–5643 (2009).
17. Vetrone, F., Boyer, J-C., Capobianco, J. A., Speghini, A. & Bettinelli, M. Significance of Yb^{3+} concentration on the upconversion mechanisms in codoped Y_2O_3:Er^{3+}, Yb^{3+} nanocrystals. *J. Appl. Phys.* **96,** 661–667 (2004).
18. Krämer, K. W., Biner, D., Frei, G., Güdel, H. U., Hehlen, M. P. & Lüthi, S. R. Hexagonal sodium yttrium fluoride based green and blue emitting upconversion phosphors. *Chem. Mater.* **16,** 1244–1251 (2004).
19. Mai, H., Zhang, Y., Si, R., Yan, Z., Sun, L., You, L. & Yan, C. High-quality sodium rare-earth fluoride nanocrystals: Controlled synthesis and optical properties. *J. Am. Chem. Soc.* **128,** 6426–6436 (2006).
20. Wang, G., Peng, Q. & Li, Y. Upconversion luminescence of monodisperse CaF_2:Yb^{3+}/Er^{3+} nanocrystals. *J. Am. Chem. Soc.* **131,** 14200–14201 (2009).
21. Berdowski, P. & Blasse, G. Luminescence and energy migration in a two-dimensional system–$NaEuTiO_4$. *J. Lumin.* **29,** 243–260 (1984).
22. Buijs, M. & Blasse, G. Luminescence and energy migration in a one-dimensional system–$EuMgB_5O_{10}$. *J. Lumin.* **34,** 263–278 (1986).
23. Danielson, E. *et al.* A rare-earth phosphor containing one-dimensional chains identified through combinatorial methods. *Science* **279,** 837–839 (1998).

24. Ananias, D. *et al.* Molecule-like Eu^{3+}-dimers embedded in an extended system exhibit unique photoluminescence properties. *J. Am. Chem. Soc.* **131,** 8620–8626 (2009).
25. Waber, J. T. & Cromer, D. T. Orbital radii of atoms and ions. *J. Chem. Phys.* **42,** 4116–4123 (1965).
26. Malta, O. L. Mechanisms of non-radiative energy transfer involving lanthanide ions revisited. *J. Non-Cryst. Solids.* **354,** 4770–4776 (2008).
27. Debasu, M. L., Ananias, D., Rocha, J., Malta, O. L. & Carlos, L. D. Energy-transfer from Gd(III) to Tb(III) in $(Gd,Yb,Tb)PO_4$ nanocrystals. *Phys. Chem. Chem. Phys.* **15,** 15565–15571 (2013).
28. Coleman, J. E. Structure and mechanism of alkaline phosphatase. *Annu. Rev. Biophys. Biomol. Struct.* **21,** 441–483 (1992).
29. Kamiya, M., Urano, Y., Ebata, N., Yamamoto, M., Kosuge, J. & Nagano, T. Extension of the applicable range of fluorescein: A fluorescein-based probe for western blot analysis. *Angew. Chem. Int. Ed.* **44,** 5439–5441 (2005).
30. Jia, L., Xu, J., Li, D., Pang, S., Fang, Y., Song, Z. & Ji, J. Fluorescence detection of alkaline phosphatase activity with β-cyclodextrin-modified quantum dots. *Chem. Commun.* **46,** 7166–7168 (2010).
31. Zhou, J., Liu, Z. & Li, F. Upconversion nanophosphors for small-animal imaging. *Chem. Soc. Rev.* **41,** 1323–1349 (2012).
32. Wang, J. *et al.* Lanthanide-doped $LiYF_4$ nanoparticles: Synthesis and multicolor upconversion tuning. *C. R. Chim.* **13,** 731–736 (2010).

Acknowledgements

The bulk of the work was supported by the Institute of Materials Research and Engineering (IMRE/12-8C0101) and the Singapore Ministry of Education (MOE2010-T2-1-083). Y.H. is grateful to KAUST Global Collaborative Research for the Academic Excellence Alliance (AEA) fund and P.Z. acknowledges the financial support from NSERC Canada. The PNC/XSD facilities at the Advanced Photon Source are supported by the US Department of Energy (DOE)-Basic Energy Sciences, a Major Resources Support grant from NSERC, the University of Washington, the Canadian Light Source, and the Advanced Photon Source. Use of the Advanced Photon Source was supported by the US DOE under contract no. DE-AC02-06CH11357. We thank PNC/XSD staff beamline scientist R. Gordon for synchrotron technical support. The authors thank H. Zhu, S. Animesh and R. Chen for technical assistance.

Author contributions

J.W., R.D. and X.L. conceived the project, performed the nanocrystal synthesis, and wrote the paper. M.A.M. and P.Z. performed the synchrotron experiments. Y.H. contributed to the high-resolution TEM imaging and analysis. B.C., J.Y., F.W., D.C., T.S.A.H. and G.L. provided input into the design of the experiments and the preparation of the manuscript.

Additional information

Supplementary information is available in the online version of the paper. Reprints and permissions information is available online at www.nature.com/reprints. Correspondence and requests for materials should be addressed to X.L.

Competing financial interests

The authors declare no competing financial interests.